POST-BUCKLING DESIGN AND TESTING OF COMPOSITE STIFFENED CYLINDRICAL SHELLS UNDER TORSION

L. Lanzi*, C. Bisagni and P. Cordisco
Dipartimento di Ingegneria Aerospaziale – Politecnico di Milano.
Via La Masa 34, 20156 Milano, Italy.

Abstract

This work is mainly devoted to the investigation of the torsional behaviour of composite stiffened cylindrical shells throughout the post-buckling field until collapse. The structures are designed to work in the post-buckling field both under axial compression and torsion without important snap-through until collapse. Besides, high ratios between collapse load and first buckling load have to be achieved.
The effects of dimensions, number and lay-up of the stiffeners are numerically investigated. Advantages offered by external reinforcing rings are explored and discussed by means of numerical analyses. The final configuration is manufactured by AGUSTA in two specimens with the same nominal characteristics.
The specimens are then tested under torsion until collapse at the Dipartimento di Ingegneria Aerospaziale of Politecnico di Milano by means of an ad-hoc testing equipment. Considerations on the post-buckling behaviour and failure mechanisms leading to collapse are discussed out. Structural collapse seems mainly due to the separation between the external reinforcing ring and the cylinder skin followed by breakage of the skin and stiffeners. Experimental results and numerical analyses are finally compared both in terms of the torque-rotation curves and of the post-buckling deformed patterns.

Introduction

Stiffened shells are structural typologies largely used in the aerospace field due to their structural efficiency in terms of stiffness/weight and strength/weight ratios. Applications of aluminium alloy stiffened shells in primary structures of aircraft fuselages, helicopter tails, wing boxes and rockets are but a few examples.

*Corresponding author:
E-mail: luca.lanzi@polimi.it
Fax: +39 02 2399.8334

In fact, if properly designed (Ref 1-2), these structures show high load capabilities, significantly exceeding the first skin buckling load.
Nowadays much effort is devoted to replace existing aluminium alloy structures with new ones made of composite materials. In fact the higher strength-to-weight and stiffness-to-weight values offered by the use of composite materials let foresee further weight reduction without loss of safety and performance.
This consideration well explains the great number of investigations on the stability and durability of composite stiffened shells carried out during the last decade. Several works (Ref 3-6) deal with the post-buckling behaviour of stiffened shells under axial compression loads considering different aspects such as collapse/failure modalities, repeated buckling behaviour, analytical-experimental correlation and design procedures; few of these works consider torsion behaviour in post the buckling field (Ref 7-9). As a matter of fact, the design of these structures should be based on detailed finite element analyses tuned and validated by means of experimental tests due to the lack of design procedures up to now available.
In particular, this work is oriented at investigating the torsion behaviour of composite stiffened cylinder shells throughout the post-buckling field until collapse. It belongs to a larger research project called "*POSICOSS* – Improved Post-buckling Simulation for Design of Fibre Composite Stiffened Fuselage Structures" and supported by the European Commission. The research project aims to obtain reliable data and to improve the knowledge of buckling and post-buckling fields of composite stiffened structures.
The data obtained shall be used in the near future to design and manufacture new generations of structures using composite materials.
In this study, a numerical and experimental investigation of the buckling and post-buckling

behaviour of thin-walled cylindrical shells made of carbon fibre reinforced plastic (CFRP) is presented and discussed.

Design of the cylindrical shell configuration

The structural typology analyzed in this work consists of cylindrical stiffened shells made of carbon fiber reinforced plastic (CFRP) woven and manufactured by AGUSTA. The material properties, reported in Table 1, are obtained by means of experimental tests on small specimens performed at the Dipartimento di Ingegneria Aerospaziale of Politecnico di Milano according to the IEPG-CTP-TA21 guidelines (Ref 10).

Table 1. Material properties

		Value
Young's modulus E_{11}	$[N/mm^2]$	57765
Young's modulus E_{22}	$[N/mm^2]$	53686
Shear modulus G_{12}	$[N/mm^2]$	3065
Poisson's ratio ν_{12}		0.048
Density ρ	$[kg/m^3]$	1510
Ply thickness	*[mm]*	0.330

The cylinder have a free length of 540 *mm* and an internal diameter of 700 *mm*. The skin lay-up consists of three [45°/0°/-45°] oriented layers, where the 0° direction is assumed parallel to the cylinder axis. Reinforced skin areas of 40 *mm* are placed on the external skin surface in correspondence of the stiffeners and made by adding three [45°/-45°/45°] oriented layers.
L-shape stiffeners, having blades of 25 *mm* and parts in contact with the skin of 32 *mm*, are bonded and riveted on the inner surface of the cylinder, in correspondence of the reinforced areas.
The stiffeners, equally spaced and equally oriented, have a rounded corner with a mean radius of about 7 *mm* due to manufacture process. A typical cylindrical configuration is shown in Figure 1.A.
Since one of the major objective of the *POSICOSS* research project is the design and testing of stiffened shells in composite materials able to work in post-buckling field, the number of stiffeners and their lay-up are optimized as so to guarantee a local skin buckling between the stiffeners and by an high ratio between the collapse load and first critical one.
In particular, in this work the cylinders are expressively designed to work under torsion. To achieve this objective, the presence of a central reinforcing ring, co-cured on the external surface at half height of the cylinder, as showed in Figure 1.B, is investigated.

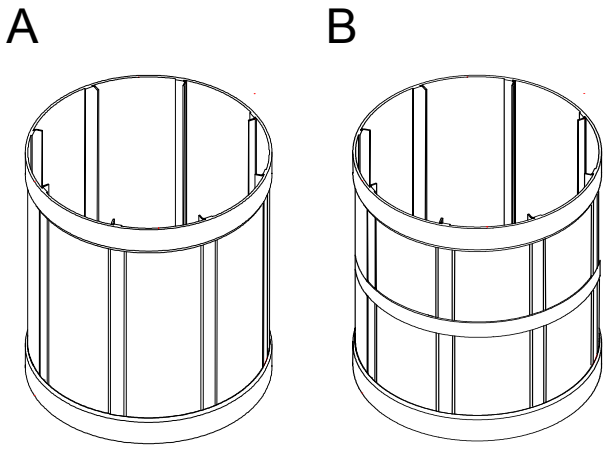

Figure 1. Typical cylindrical configurations

The design phase is mainly performed by using finite element analyses.

Finite element analyses Numerical analyses, performed using the commercial finite element code ABAQUS (Ref 11), are here used a priori to design the configuration of the stiffened cylinders. Once defined, the final configuration is manufactured by AGUSTA and then tested under torsion until collapse.
Even if the specimens are expressively designed to work under torsion, their axial compression behaviour is numerically investigated.
Basing on previous works (Ref 1,6), the design procedure is based on two different kinds of full non-linear analyses. In particular static analyses with the arch-length method proposed by Riks (Ref 12-13) and explicit dynamic analyses are used.
The arch-length method is based on the idea to follow the equilibrium path in the load-displacement

space by using as governing parameter the length of arch to cover at each iteration. The method allows to consider geometrical and material non-linearities. Herein, it is used to investigate the load-shortening curve and the evolution of buckling patterns, in terms of deformation, stress and strain, into the post-buckling field until structural collapse.
The load-displacement curves and the investigation of the deformed shape evolution from the pre-buckling to the post-buckling field until the structural collapse are also obtained by dynamic analyses.
Since dynamic analyses use equations of equilibrium which also consider inertial forces, numerical results may be affected by inertial effects due to excessively high displacement velocities.
Therefore, a good compromise between analysis results and simulated time has to be achieved.

Numerical model As far as the finite element model of the stiffened cylindrical shells is concerned, it was decided to use S4R 4-node shells, with six degrees of freedom at each node and three integration points along the thickness for each ply. After a preliminary sensitivity study on the element size, in order to prevent inaccurate results because of too coarse meshes, the dimensions of the shell elements are chosen equal to 6x6 *mm*. Therefore, the total number of shell elements in the model is equal to 36400.
A linear elastic behaviour is considered as constitutive material law.
In order to reproduce the experimental conditions of the tests as precisely as possible, finite element analyses are performed by fixing all the translational degrees of freedom of the nodes of lower edge of the cylinder. A rigid body is finally defined on the upper edge of the cylinder to which is applied the desired displacement.
Since the capabilities of composite structures to work in the post-buckling field can be significantly reduced by the presence of first localized failures which may suddenly extend producing unexpected and destructive collapse, a first ply failure approach is here adopted. Therefore first ply failures are numerically investigated using the Tsai-Hill failure criterion (Ref 14-15). According to this criterion, in-ply failures happen if the index F becomes greater than 1. Once the strength properties of the material are known, F is computed as:

$$F = \frac{\sigma_{11}^2}{\bar{\sigma}_{11}^2} - \frac{\sigma_{11} \cdot \sigma_{22}}{\bar{\sigma}_{11}^2} + \frac{\sigma_{22}^2}{\bar{\sigma}_{22}^2} + \frac{\sigma_{12}^2}{\bar{\sigma}_{12}^2} \qquad (1)$$

Since the first-ply failure hypothesis is based on the plane stress state in each lamina, it is not able to predict damage phenomena such as interlaminar cracks and/or skin-stiffeners or skin-central ring separations. Indeed it can be used as a quite conservative criterion to be applied in the preliminary design phase and to be followed, if required, by more accurate analyses an investigations.

Final configuration

The final configuration is identified after several parametric studies performed changing the number and the stacking sequence of the stiffeners in order to achieve a configuration able to work in the post-buckling field both under torsion and compression with a good residual stiffness and without important snap-through.
The final configuration is then characterized by eight stiffeners of eight $[0°/90°]_{4S}$ oriented layers.
In the following paragraphs the structural behaviour of the final configuration is numerically investigated and compared to the one expected by the same cylinder configuration without the central reinforcing ring.

Behaviour under axial compression The behaviour of the final configuration under axial compression is carried out using dynamic explicit analyses. In particular the lower edge of the cylinder is constrained while the rigid body of the upper one is moved along the axial direction with a constant displacement velocity fixed at 10 *mm/s*.
The load-shortening curves are reported in Figure 2 considering the configurations with and without the central reinforcing ring while Figure 3 shows the deformed shape evolution.
The values of the first buckling loads, of the collapse loads and of the first ply failure according to the Tsai-Hill criterion are reported in Table 2.

Table 2. Axial compression behaviour

	Without central ring	With central ring
First buckling load *[kN]*	213	217
Pre-buckling stiffness *[kN/mm]*	215	215
Elastic collapse load *[kN]*	289	---
Shortening at the elastic collapse load *[mm]*	2.37	---
First-ply failure load *[kN]*	287	310
Shortening at the first-ply failure load *[mm]*	2.42	2.80

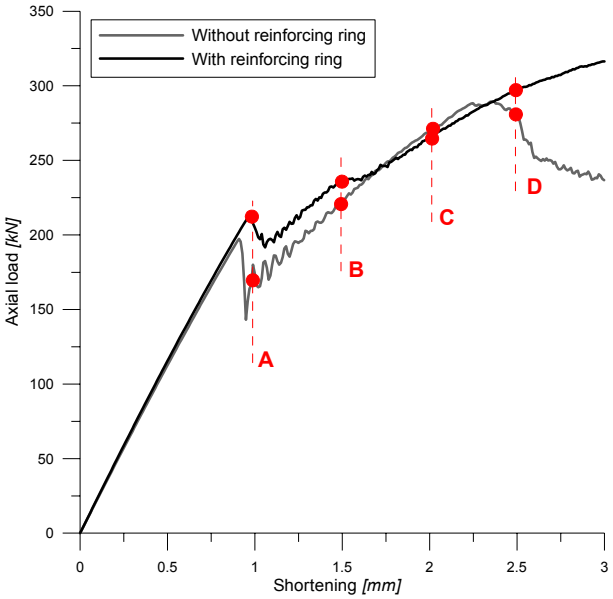

Figure 2. Load-shortening curves under axial compression

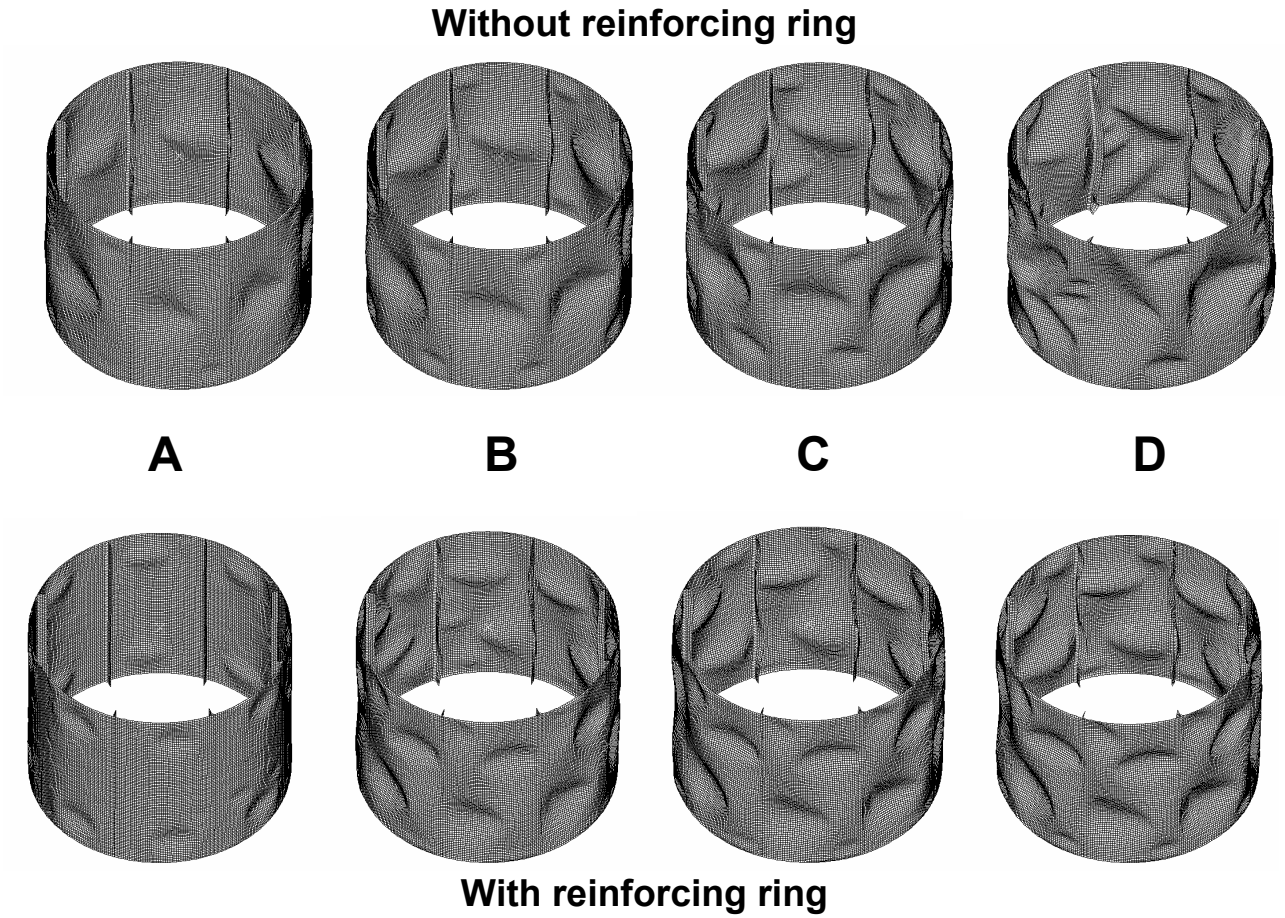

Figure 3. Deformed shape evolution under axial compression

Both the load-shortening curves and the deformed shapes show how the presence of the central reinforcing ring doesn't effect the pre-buckling behaviour of the cylinder and produces a moderate increasing of the first buckling load. On the contrary, the effects of the central ring results particularly interesting in the post-buckling field. Indeed, it seems able to significantly reduce the load snap throughout the buckling and to postpone the elastic collapse of the structure.

Behaviour under torsion The behaviour of the final configuration under torsion is investigated by means of quasi-static analyses performed with the Riks' method as well as using dynamic explicit analyses. Indeed, two different boundary conditions are considered:

1. pure torsional test conditions: a known rotation is applied to the lower edge and the upper edge is free to translate along the cylinder axis.
2. completely displacement-controlled test conditions: the only displacement allowed to the cylinder edges is a-priori known rotation applied to the lower edge of the cylinder. Consequently the axial translation of the upper edge is constrained and the axial shortening of the cylinder is forbidden.

The obtained numerical values of the first buckling load, of the collapse load and of the first ply failure according to the Tsai-Hill criterion are reported in Table 3 considering the pure torsional test and in Table 4 considering the ideal rotation-controlled one.

Table 3. Pure torsion behaviour with free axial shortening

	Without central ring	With central ring
First buckling torque *[kNm]*	13.5	17.1
Pre-buckling stiffness *[kNm/degree]*	15.8	15.8
First-ply failure load *[kNm]*	26.1	29.3
Rotation at the first-ply failure load *[degree]*	0.92	0.57

Table 4. Rotation-controlled analysis with constrained axial shortening

	Without central ring	With central ring
First buckling torque *[kNm]*	13.5	17.1
Pre-buckling stiffness *[kNm/degree]*	15.8	15.8
First-ply failure load *[kNm]*	28.0	30.8
Rotation at the first-ply failure load *[degree]*	0.73	0.47

The torque rotation curves, carried out by the Riks' method considering both the boundary conditions, are reported in Figure 4 for the configurations with and without the central reinforcing ring respectively.

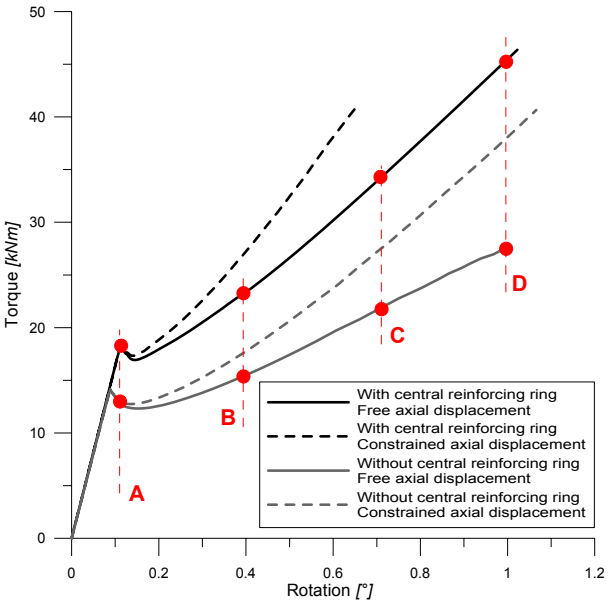

Figure 4. Load-shortening curves under torsion – Riks' method

Similar results are obtained by the dynamic explicit analyses as shown in Figure 5 limiting to the pure torsional boundary conditions where the behaviour of the configurations with and without the external reinforcing ring are compared again.

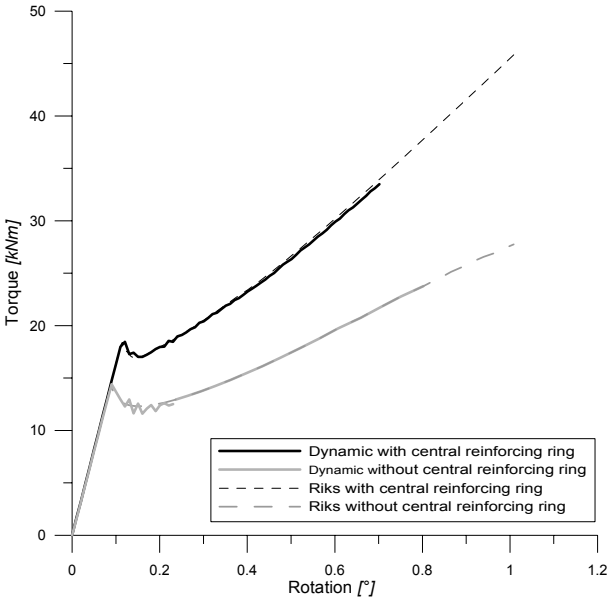

Figure 5. Load-shortening curves under torsion – Dynamic explicit analyses

Figure 6 shows the deformed shape evolution under pure torsion of the configurations without and with the central reinforcing ring obtained by the Riks' analyses.

The central reinforcing ring seems able to significantly increase the first buckling load and the torsional stiffness in the post-buckling field by radically modifying the post-buckling patterns and the stress distribution.

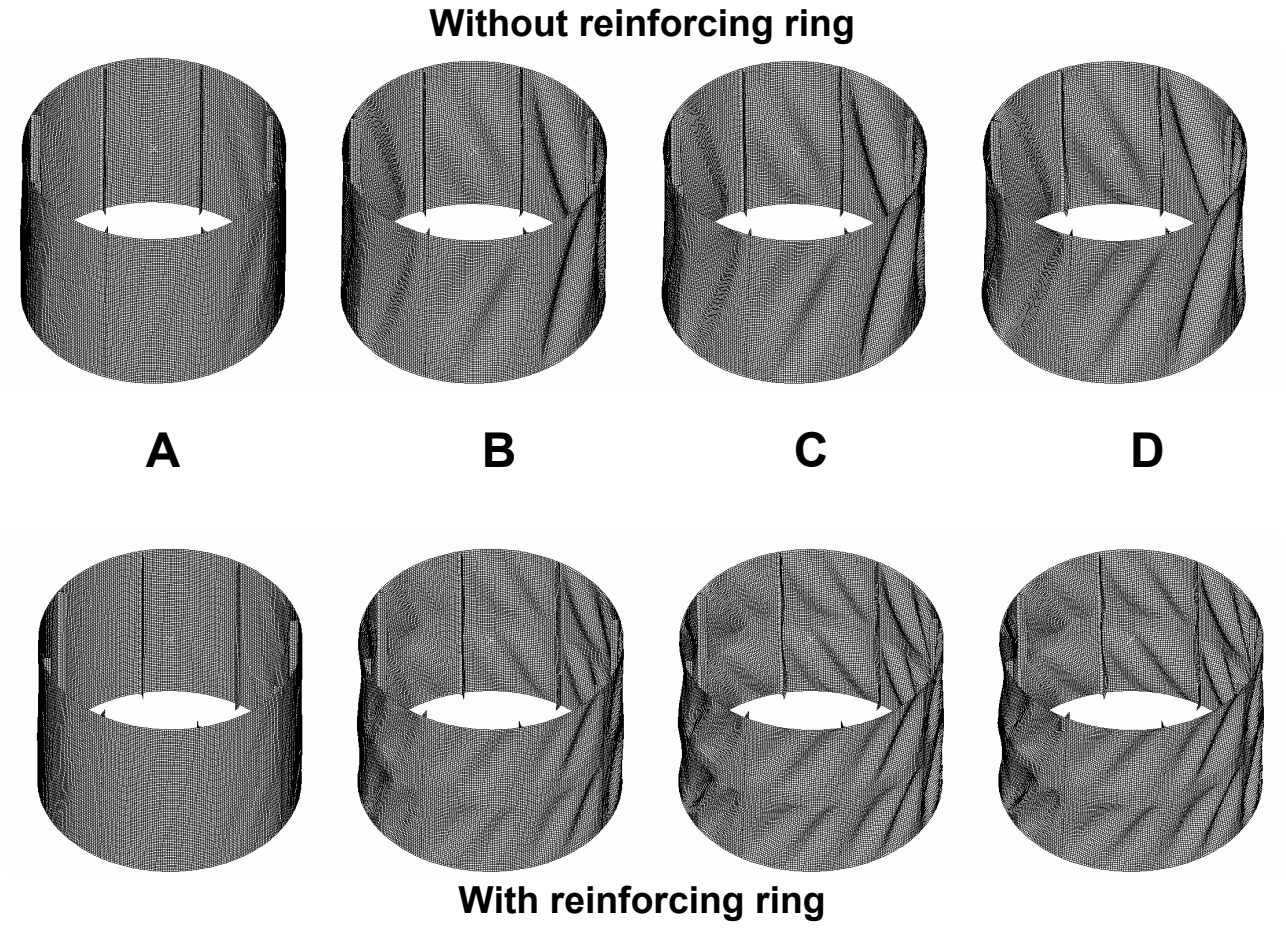

Figure 6. Deformed shape evolution under torsion

Test facility and experimental tests

Two specimens of the identified final configuration, named PE and PF, are then manufactured by AGUSTA.
The experimental tests of both the specimens are performed using the buckling test facility of the Dipartimento di Ingegneria Aerospaziale of Politecnico di Milano (Ref 9). The test facility, shown in the Figure 7, allows to perform buckling tests under axial compression as well as under torsion.

Figure 7. Buckling test facility with a cylindrical specimen inside

The facility mainly consists of two loading platforms into which the specimens are clamped. A load cell, located under the lower loading platform, is used to measure both axial and torsional loads.
Indeed, during axial compression tests, the load is provided by a hydraulic system to the upper platform that is supported by four load distribution systems placed at its four corners and made up by ball screws and stepping motors.
At the beginning of the test, the axial load is completely carried by the four screws. Then, controlling the screws by the stepping motors, the desired axial displacement is reached on the upper loading platform. Therefore part of the load is transferred to the cylinder and monitored by the load cell. The axial displacement of the specimen is monitored by using equally spaced LVDT transducers. During torsion tests, the lower loading platform is rotated using a computer-controlled torsion lever. In this case, the torsion load is directly applied to the platform while the rotation angle is computed on the base of the tangential displacement of the loading platform measured by using other three LVDT transducers.
The inner surface of the specimens are measured by means of an optical system consisting of five laser displacement sensors together working providing a resolution of 15 μm. The time required to measure the whole inner surface is limited up to 4 minutes. The data are digitally analyzed as so to represent the surface by a regular grid of points having distance of 10 *mm* in axial direction and 0.5 *mm* in the circumferential one.
As originally planned, the specimens PE and PF are tested until collapse. In order to perform completely displacement-controlled tests, it was decided to constraint the axial displacement of the upper loading platform and to apply a controlled rotation to the lower one. Since the axial shortening of the cylinders is constrained, a traction load is expected increasing the rotation angle.

Collapse test of the specimen PE The first tested specimen is the cylinder PE.

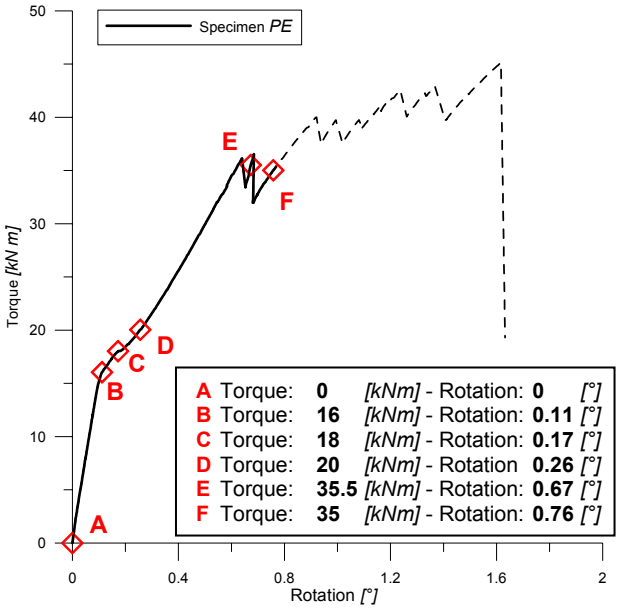

Figure 8. Torque-rotation curve of the specimen PE

The curve of the torque versus the rotation angle is reported in Figure 8 together with some highlighted points in which the internal surface of the cylinder is measured.
The measured surfaces are reported in Figure 9 and Figure 10.
The first buckling pattern is very similar to the one predicted by the numerical analyses and it is characterized by two small diagonal waves in each cylinder sector delimited by two next stiffeners in the circumferential direction and by the external reinforcing ring in the axial direction.

The first waves appear at a torsional load of 15.3 *kNm* and are limited to three of the eight cylinder bays. Once the applied torque reaches the value of 18 *kNm*, the first buckling pattern results completely developed and extended to all the cylinder bays. At this torque value, the radial displacement of the buckling waves is of about 6 *mm* respect the initial configuration.
The cylinder shows a good post-buckling residual torsional stiffness. Indeed the post-buckling torsional stiffness is equal to 45 *kNm/degree* against a pre-buckling one of 153 *kNm/degree*.

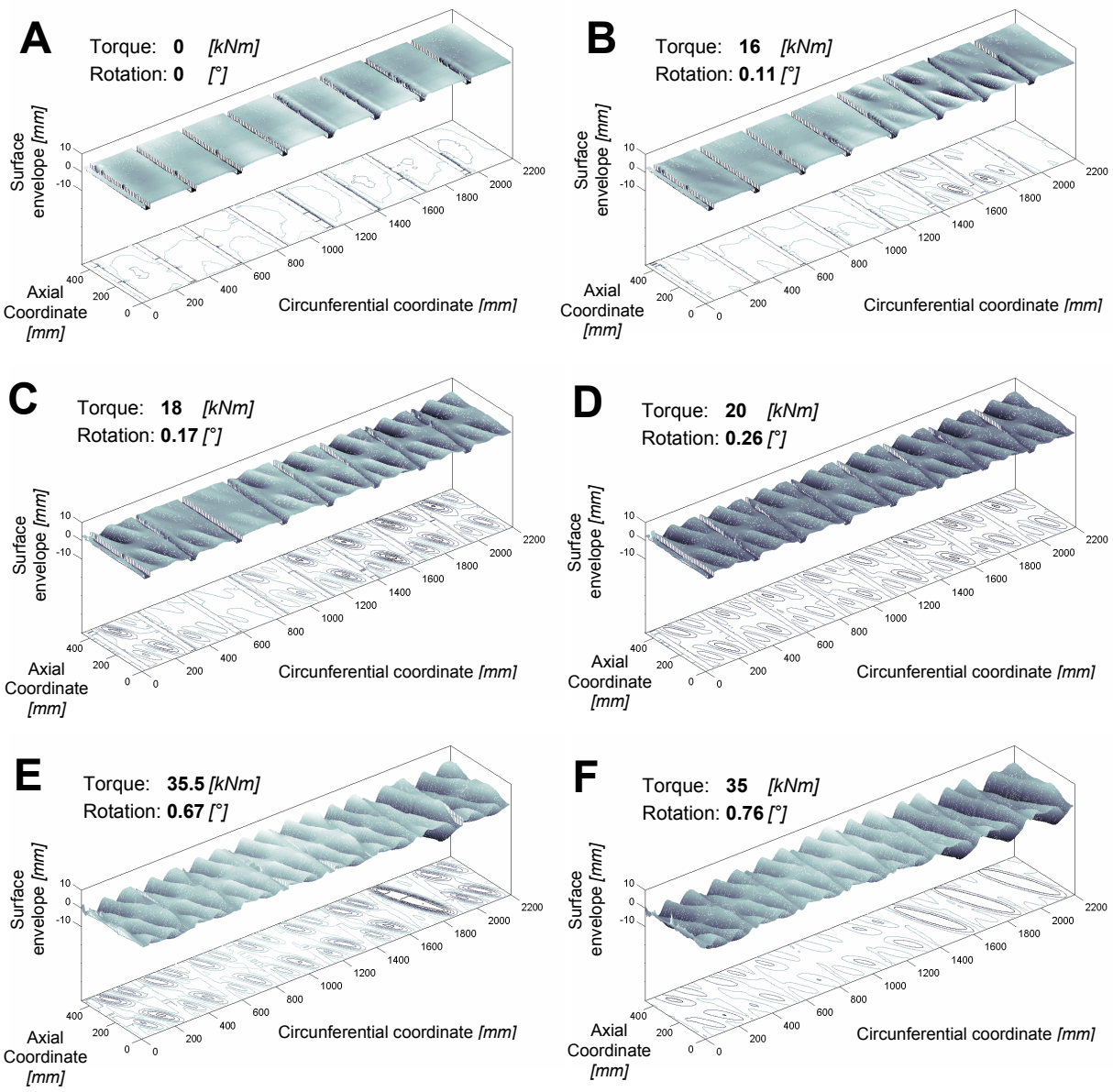

Figure 9. Internal surface envelopes of the specimen PE measured during the collapse test

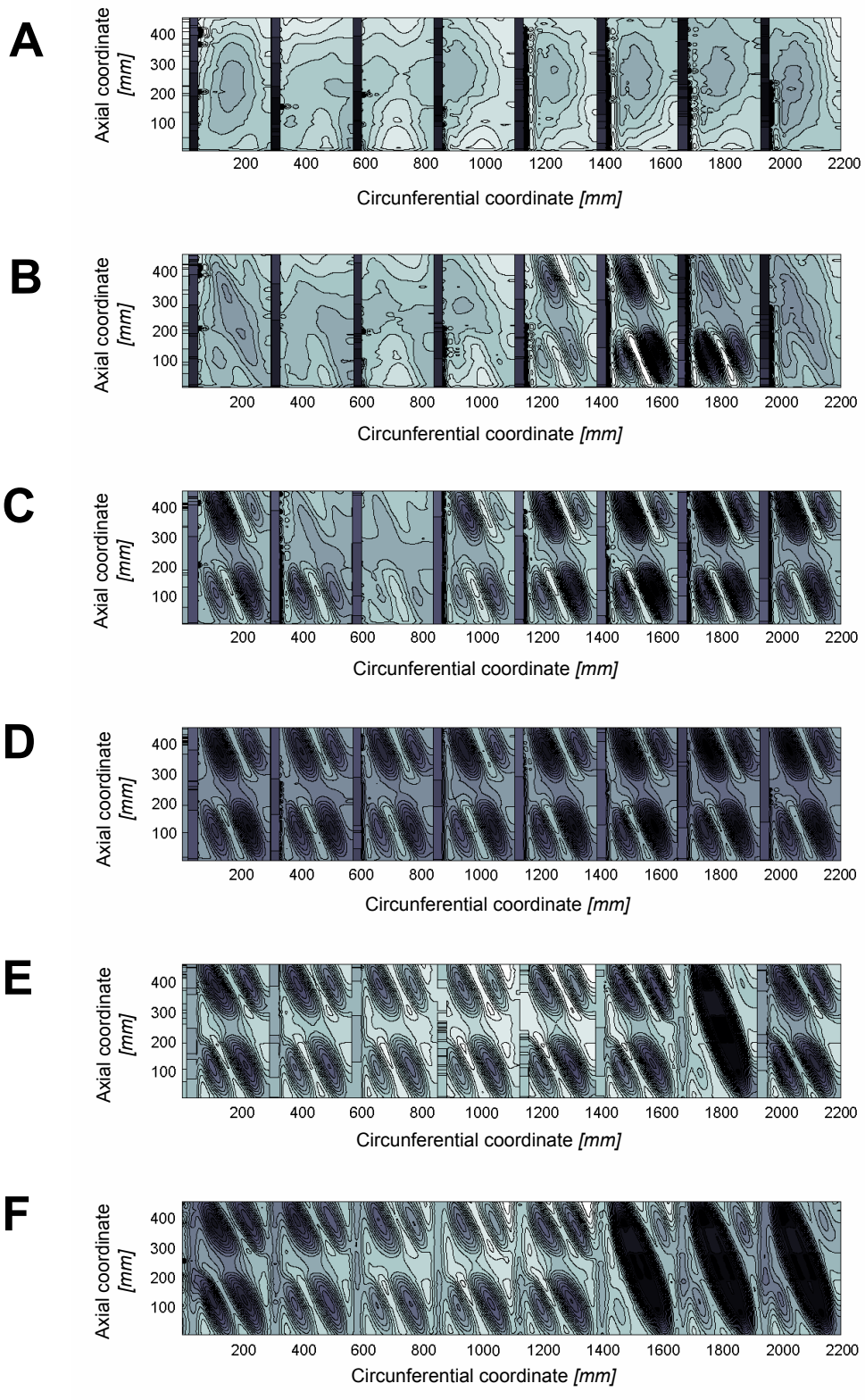

Figure 10. Contour graphs of the internal surface envelopes of the specimen PE measured during the collapse test

Once the torsional load of 35.5 *kNm* is reached, the central reinforcing ring debonds from the skin in one of the cylinder bays.
This is the direct consequence of the working modality of the skin under torsion. In fact, the post-buckling pattern of a cylinder without central reinforcing ring, as proved by numerical analyses, is characterized by ideal diagonal lines from the lower-right to the upper-left corners of each bay. In this way, traction stresses are concentrated along the bay diagonal and the fibre of these skin areas are free to shorten significantly and to move internally respect the initial cylinder radius.
This working way is here prevented by the central reinforcing ring that, remaining of the same radius, constrains the panel skin to arrange along two different diagonal waves half cylinder height. Thus, increasing the torsional load, meaningful interlaminar stresses appear between the panel skin and the reinforcing ring which produce their separation. Once the central ring is debonded, the skin pattern suddenly changes, as shown in Figure 10.F.
Increasing the rotation angle further separations are observed in the other cylinder bays as the measured inner surfaces of Figures 9 - 10 and the photos of Figures 11 - 12 show.

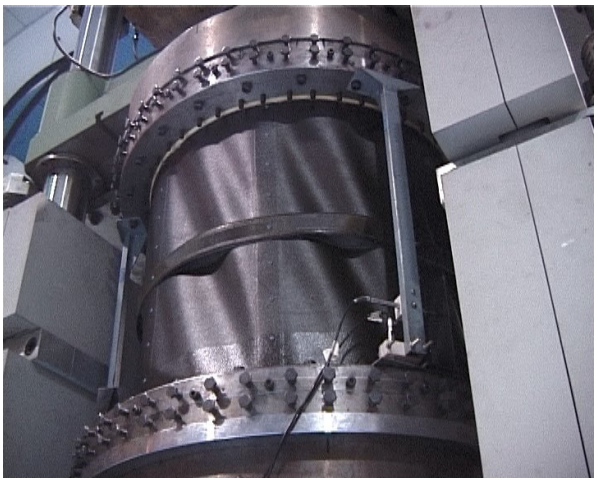

Figure 12. Particular of the debonded areas of the central reinforcing ring

The structural collapse happens at a torsional load of 45.1 *kNm* and at an imposed rotation of 1.6°.
The structural collapse involves both the panel skin and four of the eight stiffeners as showed in Figure 13. It is observed how the separation between the central ring and the cylinder skin plays an important rule in the collapse modality of the structures greatly modifying the post-buckling patterns.

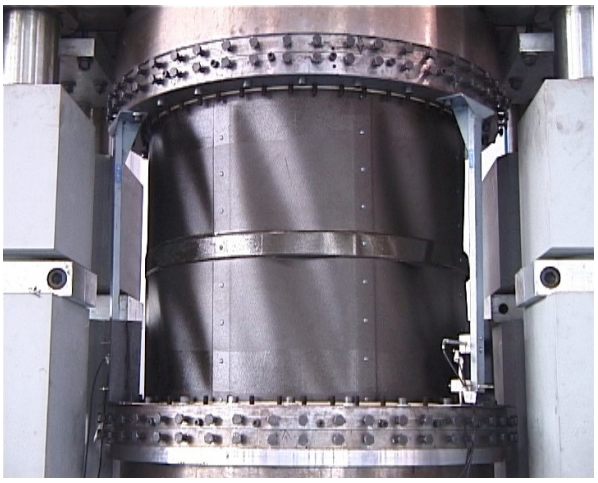

Figure 11. Post-buckling patterns due to the debonding of the central reinforcing ring

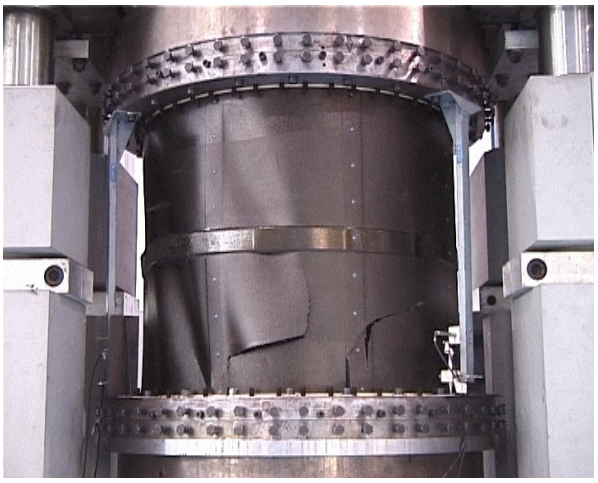

Figure 13. Particular of the specimen PE after collapse

Collapse test of the specimen PF Also the second specimen manufactured by AGUSTA is tested under torsion until collapse. The rotation is applied to the lower loading platform and the axial displacement of the specimen is constrained by fixing the upper loading platform. The torque-rotation curve of the second specimen is reported in Figure 14 while the measured values are provided in Table 5. The behaviour of the second specimen is very closed to the first one both in the pre-buckling and post-buckling fields up to the separation between the cylinder skin and the central ring. The following differences are probably due to the evolution of the skin-ring separations.

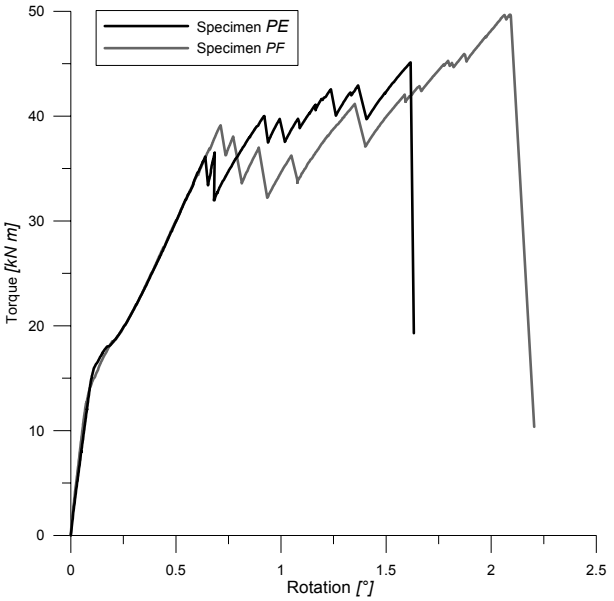

Figure 14. Comparison between the torque-rotation curves of the specimen PE and PF

Table 5. Experimental test results

	Specimen PE	Specimen PF
First buckling torque *[kNm]*	15.3	15.0
Pre-buckling stiffness *[kNm/degree]*	153	159
First skin-ring separation torque *[kNm]*	35.5	39.1
Rotation at first skin-ring separation torque *[kNm]*	0.64	0.71
Collapse torque *[kNm]*	45.1	49.6
Rotation at the structural collapse *[degree]*	1.62	2.09

Numerical-Experimental correlation under torsion

A good correlation between experimental tests and a-priori performed finite element analyses is reached in terms of the pre-buckling behaviour and of the post-buckling patterns up to the first skin-ring separation.

On the opposite, the torque-rotation curve carried out using the numerical model with the axial displacement completely constrained, as it should be happen in an ideal rotation controlled test, is a little different from the experimental one, as shown in Figure 15.

The difference can be explained considering the nature of the ideal constraint of the original numerical model by which the upper edge of the cylinder is constrained not to axially translate. This ideal constraint implies that the real test facility and the clamping systems present an infinite axial stiffness. Since this ideal hypothesis is not completely satisfied during the experimental tests of the specimen PE and PF as shown in Figure 16, where the relative axial displacement between the upper and the lower loading platforms is reported as function of the applied rotation, the original model is modified accordingly.

Therefore, in order to numerically account the effects of the finite axial stiffness, a finite stiffness in introduce by means of a spring element between the upper and the lower edges of the cylinder.

The results obtained with the enhanced model reproduce in a very accurate way the experimental behaviour until the first separation between the skin and the reinforcing ring as shown in Figure 15 and 16.

Besides, first ply failures numerically predicted happen at torque values very closed to the ones corresponding to the skin-ring separation. Therefore it can be supposed that also the stress distribution numerically obtained is in good agreement to the experimental one.

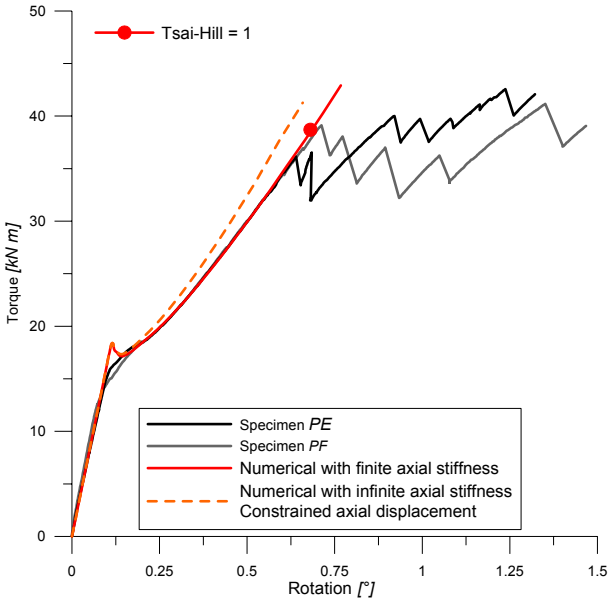

Figure 15. Numerical-Experimental correlation in terms of the torque-rotation curves

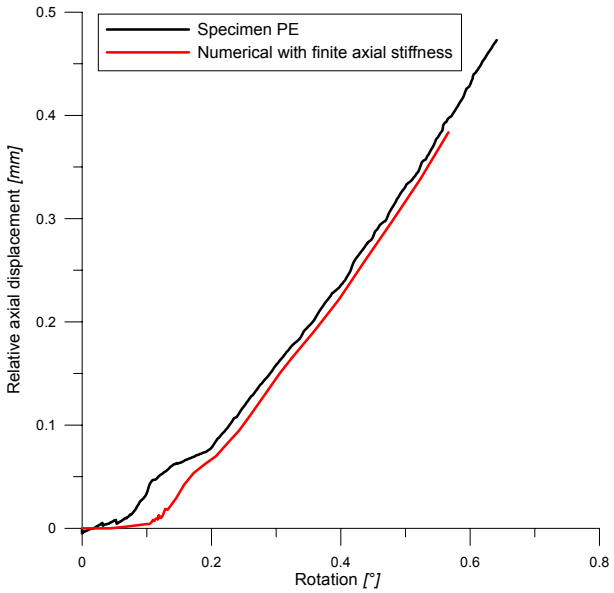

Figure 16. Relative axial displacement between the loading platforms as a function of the applied rotation

Conclusive remarks

The work presents a numerical and experimental investigation on the post-buckling behaviour of composite stiffened cylinders under torsion. The cylinders are a-priori designed by means of non-linear finite element analyses as so to work in the post-buckling field both under torsion and compression. Two different constraints and test modalities are analysed and numerically compared under torsion.

The numerical analyses show how the presence of an external reinforcing ring located at half height of the cylinder greatly improve the post-buckling performance both under compression and torsion. Indeed, it seems able to significantly reduce the load snap throughout the buckling and to postpone the elastic collapse of the structure under axial compression. It also increases the first buckling torque and the post-buckling stiffness under torsion.

Two specimens, manufactured by AGUSTA, are then tested until torsional collapse. Once reached a torque value of about 35 *kNm*, the central reinforcing ring debonds from the skin. In fact, the panel skin tries to shorten and to move internally respect the initial cylinder radius forming an ideal diagonal lines from the lower-right to the upper-left corners of each cylinder bay against the reinforcing ring that, remaining of the same radius, constrains the panel skin to arrange along two different diagonal waves half cylinder height.

The experimental data are finally compared to the numerical ones. Results appear in good agreement not only in the pre-buckling field but also in the post-buckling up to the first skin-ring separations. The differences between the first buckling loads numerically computed and the ones experimentally measured are within the 12 % and very similar post-buckling patterns are obtained.

From an industrial point of view, the research partially proves the ability of composite stiffened structures to work in the post buckling with interesting residual capabilities to carry increasing load similarly to the ones made of the aluminium alloy.

However, up to now, the lacking of extended data and consolidated design procedures makes the design of these structural typologies quite complex and time consuming requiring detailed finite element analyses tuned and validated by means of experimental tests.

Acknowledgements

The authors would like to thank Prof. Vittorio Giavotto for his generous advises. Appreciation is also extended to Agusta S.p.A. This work was partly supported by the European Commission, Competitive and Sustainable Growth Programme, Contract No. G4RD-CT-1999-00103, project POSICOSS. The information in this paper is provided as is and no guarantee or warranty is given that the information is fit for any particular purpose. The user thereof uses the information at its sole risk and liability.

References

1. Lanzi L, Bisagni C. *"Minimum weight optimization of composite stiffened panels using neural networks"*. AIAA 2003-1698, 2003.

2. Lillico M, Butler R, Hunt GW, Watson A, Kennedy D, Williams FW. *"Optimum design and testing of a post-buckled stiffened panel"*. AIAA-2000-1659, 2000.

3. Simites GJ. *"Buckling and postbuckling of imperfect cylindrical shells: a review"*. Applied Mechanics Reviews 1986;39(10):1517-1524.

4. Singer J, Arbocz J, Weller T. *"Buckling Experiments: Experimental Methods of Thin-Walled Structures"*, Vol. 1, John Wiley & Sons, New York, 1998.

5. Weller T, Singer J. *"Durability of stiffened composite panels under repeated buckling"*. International Journal of Solids Structures 1990; 26(9):1037-1069.

6. Bisagni C. *"Numerical analysis and experimental correlation of composite shell buckling and post-buckling"*. Composites: Part B 2000; 31:655-667.

7. Meyer-Piening H-R, Farshad M, Geier B, Zimmermann R. *"Buckling loads of CFRP composite cylinders under combined axial and torsion loading – experiments and computations"*. Composite Structures 2001; 53:427-435.

8. Lennon RF, Das PK. *"Torsional buckling behavior of stiffened cylinders under combined loading"*. Thin-Walled Structures 2000; 38: 229-245.

9. Bisagni C. *"Compression and torsion buckling tests on fiber composite cylinders"*. Proceedings of the 27th European Rotorcraft Forum, 11-14 September 2001, 47.1-47.10.

10. IEPG-CTP-TA 21 guidelines, Collection of Test Methods and Related Tools, 1989.

11 ABAQUS Theory and users' manuals. Hibbitt, Karlsson & Sorensen. Pawtucket U.S.A. 1998.

12. Riks E. *"An incremental approach to the solution of snapping and buckling problems"*. Int. J. of Solids and Structures 1979;15:529-551.

13. Riks E. *"The application of Newton's method to the problem of elastic stability"*. J. of Applied Mechanics 1972; 39:1060-1065.

14. Naik NK, Chandra Sekher Y, Meduri S. *"Damage in woven-fabric composites subjected to low-velocity impact"*. Composites Science and Technology 2000;60(5):731-744.

15. Singh SB, Kumar A. *"Postbuckling response and strength of laminates under combined in-plane loads"*. Composites Science and Technology 1999;59(5):727-736.